J. Fluid Mech. (2001), *vol.* 444, *pp.* 151–174. Printed in the United Kingdom

An experiment on two aspects of the interaction between strain and vorticity

By BRUNO ANDREOTTI, STÉPHANE DOUADY AND YVES COUDER

Laboratoire de Physique Statistique de l'Ecole Normale Supérieure associé au CNRS et aux Universités Paris 6 et 7, 24 rue Lhomond, 75231 Paris cedex 05, France

(Received 13 July 2000 and in revised form 11 April 2001)

Presented here are two results concerning the interaction between vorticity and strain. Both are obtained experimentally by investigating the hyperbolic flow created in Taylor's four-roll mill. It is first shown that this pure straining flow becomes intrinsically unstable through a supercritical bifurcation to form an array of counter-rotating vortices aligned in the stretching direction. The dimensionless parameter characterizing the flow is the internal Reynolds number $Re = \gamma\Delta^2/\nu$ based on the velocity gradient γ and on the gap between the rollers Δ, and the threshold value is $Re_c = 17$. Near the threshold, the transverse velocity profiles of these vortices are in excellent agreement with those predicted by the theory of Kerr & Dold (1994) in the case of an infinite hyperbolic flow. A second result is obtained at high Reynolds number. Measurements of the velocity profile in the direction parallel to the vortices show that the velocity gradient (the stretching) is systematically weaker inside the vortices than elsewhere. This demonstrates experimentally the existence of a negative feedback of rotation on stretching. This effect is ascribed to the two-dimensionalization due to the vortex fast rotation. An implication of these results for turbulent flows is a nonlinear limitation of the vorticity stretching, an effect characterized recently by Ohkitani 1998.

1. Introduction

The dynamics of three-dimensional turbulent flows is dominated by the interaction between strain and vorticity (Taylor 1938). Here we investigate this interaction in a model system, Taylor's four-roll mill experiment (Taylor 1934), which generates a strain-dominated hyperbolic flow.

The simplest example of a stagnation point flow belongs to the class of the two-dimensional linear flows having a velocity field of the form

$$v_x = \gamma x + \Omega y, \quad v_y = -\Omega x - \gamma y. \tag{1.1}$$

In the limit $\Omega = 0$, the flow is irrotational with hyperbolic streamlines (figure 1). Whereas many works have been devoted to the study of rotating flows (where locally $\gamma \ll \Omega$) and shear layers (where locally $\gamma \simeq \Omega$), stretching flows ($\Omega \simeq 0$) have received relatively less attention from experimentalists, essentially because they are difficult to generate and control.

The different investigations of the stability of three-dimensional stagnation point flows can be classified into two distinct categories. Most works (see for instance Criminale, Jackon & Lasseigne 1994 and references therein) are devoted to the

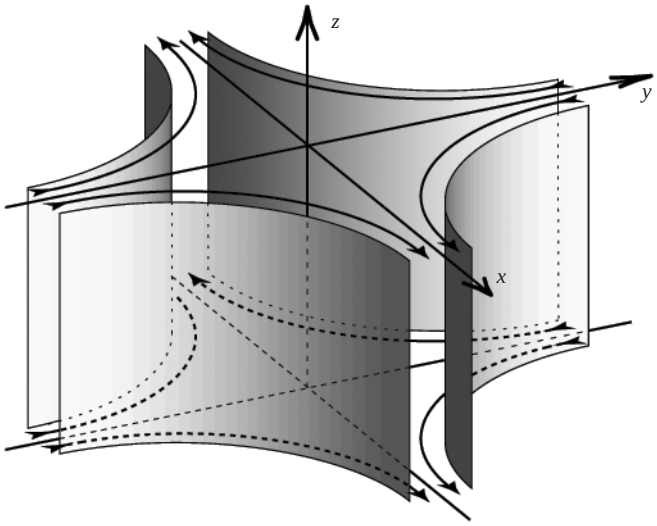

FIGURE 1. The flow near an ideal stagnation line and the axes of reference used in this work.

problem of stagnation points located at boundaries. Others deal with the stability of free stagnation lines located in the bulk of a fluid, the problem we are concerned with in the present article.

The stability of such flows was investigated by several groups motivated by two very different contexts. At very low values of the Reynolds number a hyperbolic flow can be used to study e.g. the deformation of viscous drops subjected to a pure strain. This was first carried out by G. I. Taylor in 1934. He showed that an excellent approximation of a hyperbolic flow was obtained in the space located between four counter-rotating cylinders, a geometry now called Taylor's four-roll mill experiment. This type of device has been used in various instances where a pure extensional flow was needed. Such was the case for instance in the investigation of viscoelastic fluids or in the study of the change of macromolecule conformation (Fuller *et al.* 1980; Bentley & Leal 1986; Dunlap & Leal 1987). For the practical use of such devices it is important to know in which domain of velocity the two-dimensional flow exists. A linear stability analysis was achieved by Lagnado, Phan Thien & Leal (1984). In the case of the pure extensional flow they concluded that the flow was unconditionally unstable. For each flow strength they found a lower limit to the wavelength of the unstable modes. This was in agreement with an earlier theoretical work on the stability of colliding flows by Aryshev, Golovin & Ershin (1982) and also with results obtained in the rapid distortion theory (Townsend 1976; Leblanc & Godeferd 1999). Recently Kerr & Dold (1994) revisited this problem and showed that taking into account the nonlinear terms there exist steady states which are exact (although non-analytical) solutions of the Navier–Stokes equations. They are characterized by a series of alternate vortices aligned in the extensional direction x of the flow.

Other studies were performed in the context of mixing layers. In this type of flow, primary two-dimensional eddies are generated by the Kelvin–Helmholtz instability. Each of them is separated from its neighbours by stagnation lines around which secondary streamwise vortices appear. Lin & Corcos (1984) and Neu (1984) showed that the primary vortices were subjected to a three-dimensional destabilization which generated a small amount of streamwise vorticity. This vorticity, amplified by the

stretching in the stagnation regions, rolls up into periodic streamwise alternate vortices. This situation has been simulated experimentally by the flow between two rollers, and has been captured on video by P. Carlotti, S. Obled & H. K. Moffatt (1998, personal communication).

Our interest in hyperbolic flows is due to yet another reason. It is related to the interaction between stretching and rotation in fully developed turbulence and in particular to the relation between pressure fluctuations and coherent structures. Though they may appear remote from the problem at hand it is worth summarizing briefly some results in this field.

The local structure of a turbulent flow can be characterized by the spatial distribution of strain tensor $\sigma_{ij} = (\partial_i v_j + \partial_j v_i)/2$ and vorticity $\boldsymbol{\omega} = \nabla \times \boldsymbol{v}$. The evolution in time of the vorticity ω_i is governed by the equation

$$\partial_t \omega_i + v_j \partial_j \omega_i = \sigma_{ij} \omega_j + \nu \partial_j \partial_j \omega_i \tag{1.2}$$

where ν is the kinematic viscosity. The term $\sigma_{ij}\omega_i$ means that vorticity is amplified by a longitudinal stretching, corresponding to the conservation of angular momentum. This phenomenon, which is thought to dominate the dynamics of 3D turbulence, is not yet well described in terms of elementary processes. The situation is complicated because the strain tensor obeys an even more complex equation of evolution (Ohkitani & Kishiba 1995). It is not only advected and damped by viscosity but also evolves under the complicated effects of vorticity, strain and pressure. The equation governing its evolution is

$$\partial_t \sigma_{ij} + v_j \partial_j \sigma_{ij} = \tfrac{1}{4}(\omega_k \omega_k \delta_{ij} - \omega_i \omega_j) - \sigma_{ik}\sigma_{kj} - \partial_{ij} p + \nu \partial_j \partial_j \sigma_{ij}. \tag{1.3}$$

It is crucial to note that (1.3) is a non-local equation since pressure depends on the whole flow (in particular on boundary conditions) through the Poisson law

$$\Delta p = \tfrac{1}{2}\omega_i \omega_i - \sigma_{ij}\sigma_{ij}. \tag{1.4}$$

In reverse, relation (1.4) means that pressure measurements can be used to investigate the spatial distribution of vorticity and strain. The existence of low-pressure filaments in turbulent flows was demonstrated experimentally by Douady, Coudet & Brachet (1991). They correspond to rotating regions in which the vorticity is concentrated in a thin core while the strain is spread at the periphery, as in a Burgers vortex (Burgers 1940). Correspondingly the fluctuations of pressure at one point were investigated by Fauve, Laroche & Castaing (1993) and Cadot, Doudy & Couder (1995). Generally in these experiments as well as in previous numerical simulations (Brachet 1991; Métais & Lesieur 1992) the probability distribution function of pressure exhibits a strong asymmetry with a long exponential tail towards the low pressures and a shorter Gaussian tail towards the high pressures. The low-pressure troughs are the signature of filaments passing the probe. The absence of corresponding high-pressure peaks is a clue pointing to the absence of organized high strain regions.

Numerical simulations permit direct observation of the structures present in turbulent flows. Since the initial work by Siggia (1981) a specific effort has been devoted to the detection of vortices in simulations of increasing spatial resolution (Jimenez *et al.* 1993; Jeong & Hussain 1995; Kida & Miura 1998). More generally the spatial distribution of enstrophy $\omega^2 = \omega_i \omega_i$ and strain modulus $\sigma^2 = 2\sigma_{ij}\sigma_{ij}$ were investigated by Tanaka & Kida (1993); Jimenez *et al.* (1993); Tsinober *et al.* (1997); Tsinober (1998); Nomura & Post (1999). The joined probability density functions show that there exist regions in which the vorticity is large and the strain small. When these regions are singled out, they appear in the form of filaments. Similarly the regions

where both ω^2 and σ^2 are large are observed to be in the shape of sheets. Finally, the regions of large σ^2 and small ω^2 are far less probable and have no specific spatial structure.

The first question that motivated the present work is thus: why are there no organized regions of high strain and weak vorticity, i.e. no high-pressure structures? The observations in the mixing layers suggest that this is linked with the instability of hyperbolic regions. In between the main eddies there are stagnation lines which should be high-pressure regions. Instead it is well known that this is the locus of formation of secondary streamwise vortices. As observed by Douady *et al.* (1991), these streamwise vortices are low-pressure filaments. The paradox is that where high pressure is expected, low-pressure filaments form.

The second question is related to the enhancement of vorticity by stretching. Does it occur mainly in strain-dominated regions or in organized vortices? In a preliminary work (Andreotti, Doudy & Couder 1997) we showed, using two distinct experiments, that the vorticity stretching occurs mostly before the vortices are formed but that the stretching decreases after their formation. This effect was ascribed by Andreotti *et al.* (1997) to the two-dimensionalization of the flow near the core of rapidly rotating vortices, an effect which results in a reduction of the longitudinal velocity gradient (Andreotti 1999). This observation is likely to be correlated with the results obtained on the statistics of enstrophy production in turbulent flows. From various conditional averaging Tsinober, Ortenberg & Shtillman (1999) have demonstrated that the enstrophy production is much larger in the regions dominated by strain than in those dominated by enstrophy.

For all these reasons we wanted to do a direct experimental investigation of the stability of a pure strain flow in a model experiment and to observe the dynamics of both stretching and vorticity in such regions. First aiming to obtain a well-controlled hyperbolic flow we were brought back to Taylor's (1938) four-roll mill experiment. There is, to our knowledge, only one previous experimental investigation of the stability in this geometrical configuration, by Lagnado & Leal (1990). They found, over a certain threshold, the formation of vortices aligned in the stretching direction. But in their experiment this array was limited to two vortices located near the extremities of the cylinders with one single recirculation vortex in between. This led them to conclude: 'the vortices are primarily an end effect and a column of alternate vortices does not appear throughout the entire vertical extent at larger aspect ratio...'. Our experiments, done in a different geometry, lead to a different conclusion.

The first part of this article deals with the instability of a hyperbolic flow at low Reynolds numbers. After a description of the experimental apparatus, we will discuss the two-dimensional stagnation point flow obtained at very low Reynolds numbers and describe its destabilization and the formation of a row of counter-rotating vortices aligned in the stretching direction.

In the second part, we investigate the interaction between stretching and rotation in the same experiment but at high Reynolds numbers. We will present evidence that there is a negative feedback of the rotation of the vortices on the stretching to which they are submitted. As a conclusion, the consequences of such a mechanism for turbulent flows will be discussed.

2. Experimental set-up

The design of a cell in which the flow has a pure strain field appears, at first sight, to be impossible. Indeed, integrating the Poisson equation (1.4), we obtain the equality

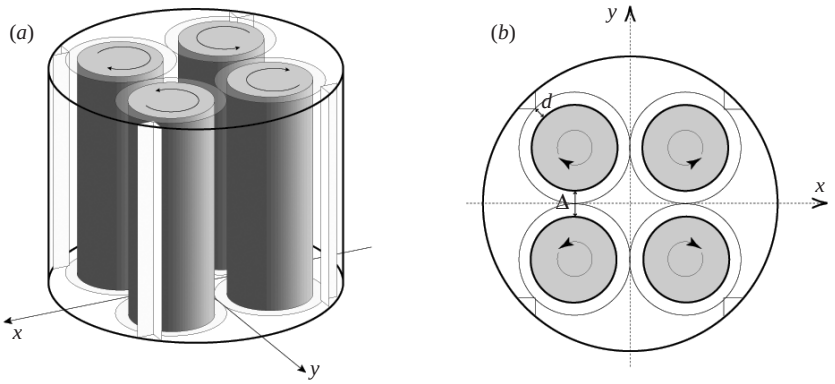

FIGURE 2. (*a*) Sketch of the experimental Taylor's four-roller mill. Two details can be seen. The cylinders are terminated by circular end plates which reduce the recirculation in this region. Four wedges are glued onto the outer boundary and reduce the minimum distance between the rollers and the cell wall to d. They avoid the formation of Taylor–Couette rollers between the cylinders and the outer walls. (*b*) Transverse section of the experimental set-up.

of enstrophy and strain, on the average:

$$\langle \omega^2 \rangle = \langle \sigma^2 \rangle. \tag{2.1}$$

In fact, as was pointed out by Raynal (1996) this relation does not necessarily hold in a closed cell having moving boundaries. This is precisely the case in the four-rollers geometry.

The core of the experiment is composed of four cylinders having parallel axes and placed at the corners of a square (figure 2). The two cylinders placed on one diagonal rotate at one velocity, the two others at a second velocity. As is well known, all the linear flows of the form (1.1) can be obtained in the central region of this apparatus when the fluid is very viscous and the rotation speed small. When the velocities of the cylinders are opposite, the flow is very close to the ideal hyperbolic flow:

$$v_x = \gamma x, \quad v_y = -\gamma y. \tag{2.2}$$

In the outer region of the cell, bounded by the container's wall, most of the flow corresponds to four halves of hyperbolic flows. Thus, globally in the whole cell the flow at low velocities is dominated by pure strain. The reason why it does not contradict equation (2.1) is that the motion of the cylinders has to be taken into account in the balance between strain and enstrophy. In these cells the vorticity could be said to be frozen inside the rotating cylinders while the strain is in the flow.

In practice, the radius R of the rollers and the gap Δ between them can be chosen at will in order to obtain the best approximation of a hyperbolic flow. The distance $(R + r)$ of the rollers axis to the centre of the cell (figure 3) is given by

$$(R + r)^2 = 2(R + \Delta/2)^2. \tag{2.3}$$

The hyperbola tangent to the rollers (figure 3) has a radius of curvature r. If R was chosen equal to r the hyperbola and the circle would have the same radius of curvature at the point of tangency. Instead, we chose empirically a value of r ($r = 29\,\text{mm}$) slightly smaller than R ($R = 35\,\text{mm}$). For these values the two curves (the circle and the hyperbola) remain close to each other in a larger region (figure 3). The minimum distance between two adjacent cylinders is thus $\Delta = 21\,\text{mm}$. The four

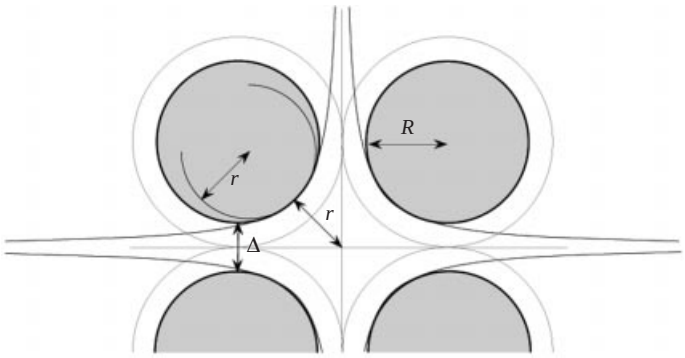

FIGURE 3. Scheme of the geometrical constraints leading to the choice of R and Δ. The radius of curvature r of the hyperbola tangent to a roller has to be slightly smaller than R.

cylinders have a length $h = 190\,\text{mm}$ so that the aspect ratio of the gap separating them is $h/\Delta \simeq 9$.

Preliminary experiments demonstrated that the main problem of the set-up for a stability study was to obtain a situation in which the inner flow was not disturbed by inhomogeneities due to the structure of the flow in the outer region of the cell. These structures are determined by the geometry of the space between the four rollers and the container. The tank can be either square or circular in section. It can also be either large compared to the central region or not. We performed several preliminary experiments using Kalleiroscope to observe the structure of the flow in the whole cell. We first eliminated the use of square containers as complex recirculations are created in their corners. However, with cylindrical containers the situation is still complex. At two locations the fluid expelled from the central region impinges on the outer wall while it is pumped back into the central region at two other locations (figure 2). Each of these four regions is half of a hyperbolic flow. They are separated from each other by regions where the fluid is located between the rotating cylinder and the external boundary. In these latter regions, the flow can be submitted to a centrifugal instability. If the gap is wide, direct observation shows the formation of Couette–Taylor-like structures in the shape of superposed sectors of tori with alternate directions of rotations. The larger the gap between the rollers and the container the lower the velocity at which these structures form. In the central region, the flow is then complex with visible arrays of tori around each of the four rollers. A natural solution to avoid this problem is to reduce the gap between the rollers and the outer wall so as to increase the velocity for which the centrifugal instability will appear. However if the four rollers are confined in too narrow a cylinder there is a drastic reduction of the flux of fluid which is necessary both as the output and the input of the hyperbolic inner flow. In such situations the flow in the central region consists of complex recirculations and is no longer hyperbolic.

For these reasons we chose an intermediate configuration with a narrow container 120 mm in radius, only leaving a minimum gap of 21 mm between the cylinders and the wall. Four protruding wedges parallel to the cylinders were glued onto the cell wall in order to reduce locally by 2 (table 1) the minimum gap d between the cylinders and the wall (figure 2). The formation of Couette structures in this region was thus inhibited. This was systematically checked by direct visualizations in the range of velocities of interest. In this configuration, below the instability threshold, the inner flow is an excellent approximation of a hyperbolic flow. We note however that the

Fluid	v ($cm^2\,s^{-1}$)	ρ ($g\,cm^{-3}$)	R (mm)	Δ (mm)	d (mm)	Anemometer	Re_c
Glycerol	0.956	1.24	35	21	15	DOP	18.8
Glycerol solution	0.154	1.24	35	21	10	PIV	15.8
Water	0.01	1	35	21	15	DOP	

TABLE 1. Characteristics of our experiments. Three viscosities v have been used. The geometrical parameters (the rollers radius R and the gap Δ between them) are kept constant and the minimum distance d between the rollers and the external boundary is varied.

reduction of the outer gap results in a reduced stirring efficiency of the rollers, as will be discussed below.

The length of the four rollers was only 5 mm shorter than that of the container. When the rollers are simple cylinders, we observe, as Lagnado & Leal (1990) before us, the formation of intense toroidal circulations at their extremities. This derives from an Eckman effect. Its rotation being slowed down by the friction on the wall, the fluid moves inwards at the extremity of a roller. In order to reduce these end effects, thin disks of (larger) radius $R + \Delta/2 = 45$ mm were added at the ends of the cylinders (figure 2 and figure 3). The end effect is then reversed and considerably reduced in intensity.

Three fluids were used in these experiments: a concentrated glycerol solution, a diluted one and pure water (table 1). A visual observation of the flow could be done using Kalleiroscope. For measurements of the velocity fields the fluid contained neutrally buoyant particles of small size (100 μm). We videotaped cross-sections of the flow lit with a planar laser beam. These images were then used in several ways. Images of streaks were obtained by integrating the video images during 0.4 s (20 frames). It was also possible to reconstruct the velocity field using the particle image velocimeter described in Cardoso, Marteau & Tabeling (1994), which uses image intercorrelation.

We also used an ultrasonic Doppler anemometer (DOP 1000 constructed by Signal Processing Co.) to measure various velocity profiles. This apparatus emits ultrasonic pulses of frequency 4 MHz and the Doppler shift of the signal retrodiffused by the passive particles gives the longitudinal component of the velocity at 114 equidistant points located along the ultrasonic beam. An 'instantaneous' profile results from the averaging of several consecutive pulses separated by a time interval of the order of 50 ms. The width of the ultrasonic beam is of the order of 2 mm and limits the spatial resolution of this technique. It is worth noting that the two anemometers (DOP and PIV) have their maximal resolution in different velocity ranges (around $100\,mm\,s^{-1}$ and $10\,mm\,s^{-1}$ respectively). We thus used the PIV method in the diluted glycerol solution and the Doppler anemometer in water and in concentrated glycerol (see table 1).

3. The instability of the hyperbolic flow: experimental results

3.1. *The basic hyperbolic flow*

Observation of the central region of the cell at low Reynolds number shows that a good approximation of a hyperbolic flow is obtained. The velocity profile $v_x(x)$ along the stretching axis x is approximately linear in the central region, the maximum being achieved between the rollers (figure 4). The shape of the velocity profile does not change much as the rollers frequency F increases and its amplitude is found to vary

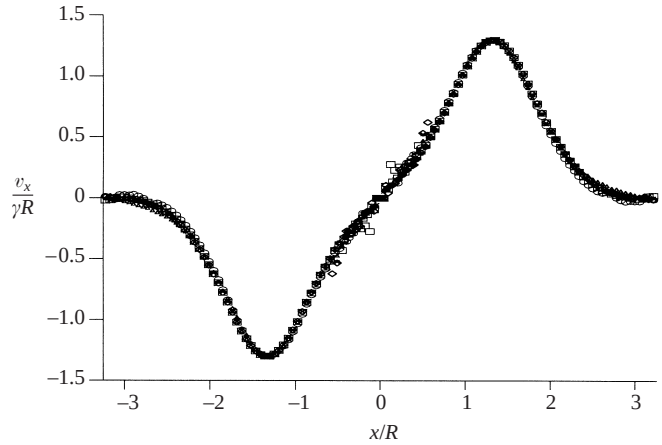

FIGURE 4. Rescaled velocity profile along the extensional axis x for various frequencies between $F = 0.5\,\mathrm{s}^{-1}$ and $F = 3\,\mathrm{s}^{-1}$, for the glycerol.

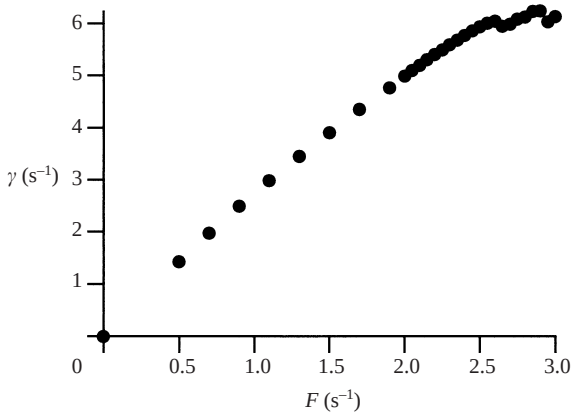

FIGURE 5. The stretching coefficient γ as a function of the roller frequency F, the working fluid being the glycerol.

proportionally to the cylinder frequency F. In particular the velocity gradient in the central region scales as F:

$$\frac{\partial v_x}{\partial x} = \gamma = kF. \tag{3.1}$$

The coefficients of proportionality in our experiments were $k = 1.4$ for the diluted glycerol solution and $k = 2.7$ for the concentrated one (figure 5). These values are approximately respectively a quarter and a half of that ($k = 5.1$) found by Taylor (1934). This difference is due to the fact that the efficiency of the rollers in setting the fluid into motion is a function of the geometry of the whole cell. In Taylor's experiment the four rollers are surrounded by a large tank. In ours the flow is forced through narrow gaps d (see table 1) between the rollers and the walls of the container, a hindrance to the stirring efficiency.

We will need a parameter to describe both the hyperbolic flow and its confinement. Because of the variation of the stirring efficiency we cannot use directly the frequency of the cylinders to describe the physical situation. In a different tank (e.g. for a

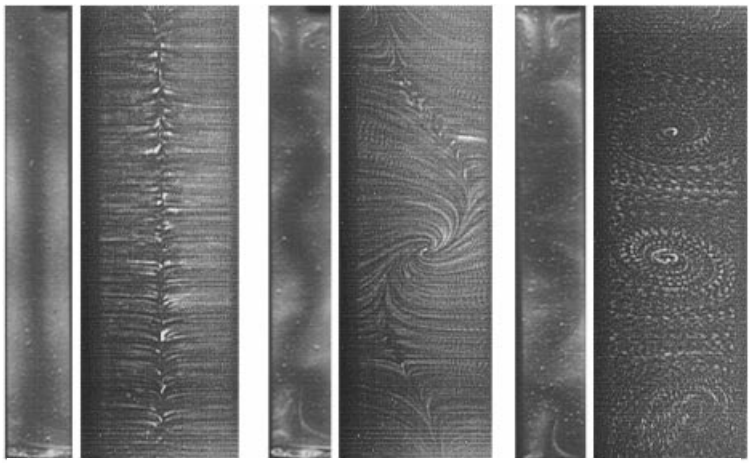

FIGURE 6. Images of cross-sections of the flow in the plane (yOz) perpendicular to the stretching, for the diluted glycerol solution. For each frequency, the whole field is shown on the left (visualization using Kalleiroscope) and a close-up view is shown on the right (visualization with spherical particles, integrating the video images for 0.4 s). (*a*) The hyperbolic flow at $F = 0.3$ Hz (or $Re = 8.7$) well below the instability. (*b*) The flow at $F = 0.55$ Hz (or $Re = 15.9$) immediately above the threshold. (*c*) The flow at $F = 0.66$ Hz (or $Re = 19.1$) with a periodic array of alternate vortices.

different parameter d) the same velocities of the cylinders produce a different flow. The best parameter to describe the actual hyperbolic flow is thus the measured fluid velocity gradient γ as given by equation (3.1). In particular, all the velocity profiles along the extensional axis x collapse once rescaled using γ (figure 4). The flow being, in the central region, geometrically bounded by the rollers themselves we will choose as the typical length scale the gap Δ between them. From these two quantities we form a Reynolds number:

$$Re = \frac{\gamma \Delta^2}{\nu}. \tag{3.2}$$

With this definition we find that below a critical value Re_c the flow is stable (figure 6*a*).

3.2. *Instability threshold*

At the critical Reynolds number $Re_c \simeq 17$, the central vertical line which separates the two colliding jets destabilizes into a sinusoid (figure 6*b*). For a slightly larger value the formation of an array of steady alternate vortices is observed (figure 6*c*). It is important to note that in this velocity range no other structure is observed in the cell. More specifically no tori due to a centrifugal instability exist near the cylinders. The observed instability affects the core of the hyperbolic flow. For this reason we are confident that the instability observed here is an intrinsic characteristic of the hyperbolic region, even though the visual evidence may appear insufficient to rule out completely any centrifugal effect. The distance separating two successive vortices in the vertical direction is of the order of the gap Δ between the cylinders. At approximately $Re \simeq 45$ the vortices become chaotic. Well-defined vortices are observed in the whole range of Reynolds numbers explored (up to 3000). It is worth noting that an internal Reynolds number of 3000 (in water) corresponds to a Reynolds number based on the rollers velocity and radius of 10^5.

Just above threshold the velocity field can be decomposed into the sum of two fields: one, $\boldsymbol{v}_\varphi$, corresponding to the stretching part of the flow, the second, $\boldsymbol{v}_\psi$, to the array of vortices. Using the cut through the flow by the laser plane, we were able to investigate the flow in several parallel planes $x = c^{st}$. It turns out that the vortices are mainly two-dimensional (invariant along x) at least in the central region. The vortical part in the plane yOz can thus be associated with a streamfunction ψ. The rest of the flow is associated to the colliding jets and corresponds to pure deformation without vorticity. It can thus be associated with a potential φ. Globally the velocity field in the central plane perpendicular to the stretching direction x is written as $\boldsymbol{v} = \boldsymbol{v}_\psi + \boldsymbol{v}_\varphi$:

$$v_y = \partial_z \psi + \partial_y \varphi, \quad v_z = -\partial_y \psi + \partial_z \varphi. \tag{3.3}$$

It should be noted that the v_x velocity component around the central plane $x = 0$ is approximately equal to $-\Delta\varphi x$. Well below the threshold the flow is purely hyperbolic and corresponds to a constant streamfunction ψ and to a quadratic potential $\varphi = -\gamma y^2/2$. In the more general case the main problem is that different sets of functions ψ and φ can be chosen corresponding to the same physical flow. Usually the particular choice of ψ and φ is imposed by the boundary conditions. Here this would be arbitrary. We thus selected the decomposition which minimizes the difference between the stretching part of the flow and a pure hyperbolic flow (between φ and $-\gamma y^2/2$). The interested reader will find the details of the decomposition method in the Appendix.

Four velocity fields are analysed in this way in figures 7 and 8. Well below the threshold (figure 7*a*) there is only a stretching component and no vorticity. Immediately below the threshold weak vortical regions appear near the extremity of the cylinders (figure 7*b*). Immediately above the threshold the main characteristic of the flow is the sinusoidal deformation of the convergence line. The decomposition of the field reveals the presence of an array of small-amplitude counter-rotating vortices (figure 8*a*). Finally, well above the threshold (figure 8*b*) the vortical component dominates the flow. The contours of iso-value of the streamfunction show that the vortices are elliptical, the large axis along y being approximately twice as long as the short one. The stretching field is no longer constant in the spanwise direction, particularly near the vortex cores.

In order to characterize the bifurcation we can use as the order parameter the maximum ψ_M of the streamfunction as a function of the Reynolds number. Its evolution (figure 9) is that of a supercritical transition. Above the threshold ψ_M varies as $(Re - Re_c)^{1/2}$. The bifurcation, however, appears imperfect as ψ_M starts growing below the threshold. This is due to the finite-amplitude perturbation created by the end effects.

We measured the critical value of the stretching using two methods, PIV anemometry and ultrasonic Doppler anemometry for the two different viscosities (see table 1) and with different configurations of the external wedges (and thus a factor of 2 in the efficiency of stirring). The critical Reynolds number Re_c is around 15.8 for the glycerol with a small gap d. It is around 18.8 for the less viscous solution and the larger gap d. In both cases, the threshold in frequency F is well defined: the difference between the two values of Re_c comes from the error on the velocity gradient and on the viscosity, and perhaps from a small geometrical effect coming from the wedges (actually from d). It is worth noting that the critical Reynolds numbers based on the roller frequency F are far from each other, being respectively 15.4 and 7.3.

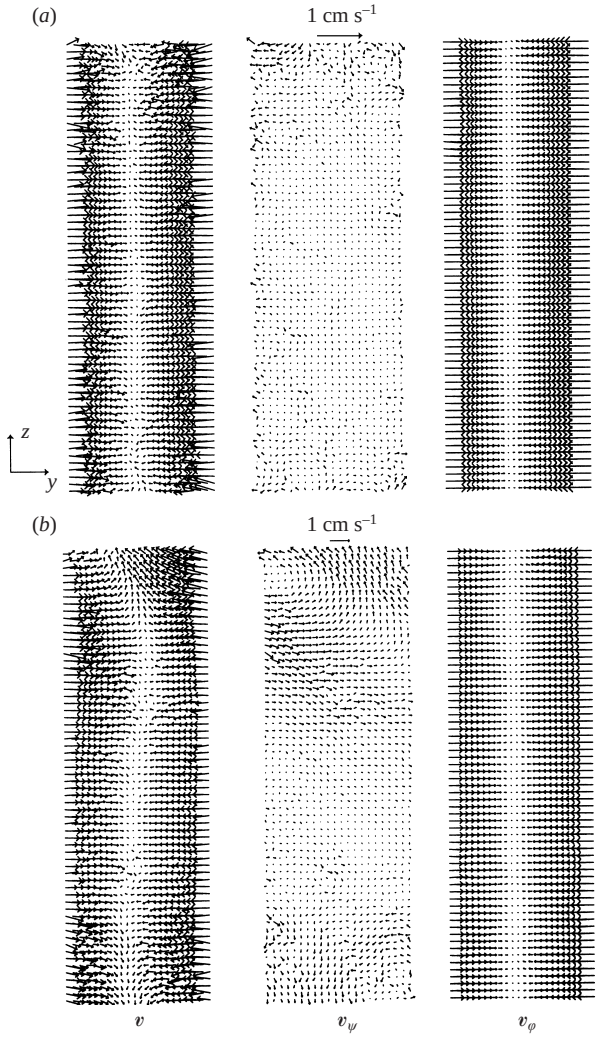

FIGURE 7. The velocity field in the plane $x = 0$ for two rotation frequencies below the instability threshold: (*a*) $F = 0.25$ Hz ($Re = 7.2$); (*b*) $F = 0.50$ Hz ($Re = 14.5$). In each case the actual velocity field $\boldsymbol{v}$ is given on the left. It is decomposed into a two-dimensional vortical component $\boldsymbol{v}_\psi$ (centre) and in an irrotational stretching part (right) $\boldsymbol{v}_\varphi$.

4. The instability of the hyperbolic flow: theoretical aspects

4.1. *Linear stability analysis*

The linear stability analysis of the idealized hyperbolic flow (2.2) shows that it is always unstable. Several variants of this analysis can be found in Aryshev *et al.* (1982); Lagnado *et al.* (1984); Craik & Criminale (1986) (who use the growth of Fourier modes), Leblanc & Godeferd (1999) (who use the rapid distortions theory), Lin & Corcos (1984), Neu (1984) and Criminale *et al.* (1994). Basically the instability is due to the amplification by stretching of vortical disturbances. This is particularly easy to see at the stagnation point where the velocity is null so that the equation governing the vorticity reduces to

$$\partial_t \omega_x = \gamma \omega_x, \quad \partial_t \omega_y = -\gamma \omega_y, \quad \partial_t \omega_z = 0. \tag{4.1}$$

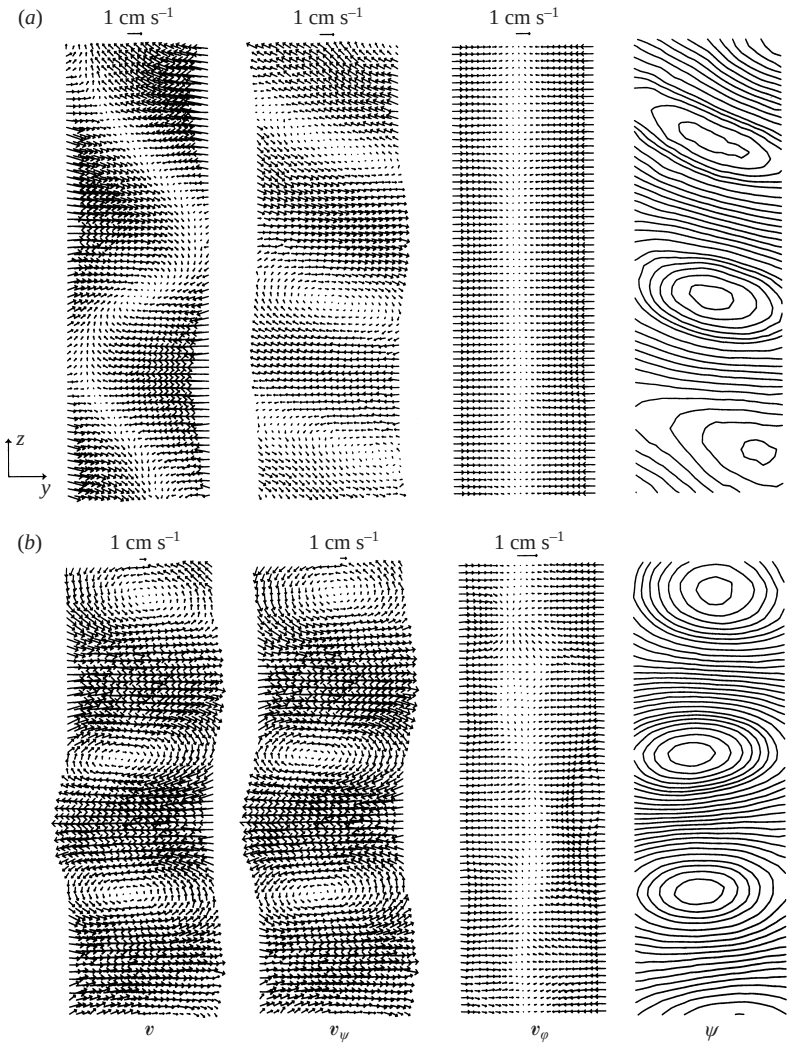

FIGURE 8. As figure 8 but for two rotation frequencies located above the threshold: (*a*) $F = 0.55$ Hz ($Re = 15.9$); (*b*) $F = 0.65$ Hz ($Re = 19.1$). The streamlines (iso ψ) are shown on the right.

Of particular interest for comparison with the experimental results is the work of Kerr & Dold (1994) who obtained by semi-analytical means a family of exact stationary solutions. They correspond to a periodic array of counter-rotating vortices aligned in the stretching direction x. The class of solution has two free parameters: the amplitude ω_0 and the wavenumber k of the fundamental mode. This calculation demonstrates that the nonlinearities do not change the flow fundamentally: the solutions of the linearized problem are very close to being exact solutions of the full Navier–Stokes equation. It should be understood that neither the amplitude nor the wavelength are selected by nonlinearities: they only induce the growth of harmonics.

For this reason we will limit ourselves here to the solutions of the linearized equations, emphasizing the parameters relevant for comparison with the experimental results. We also propose an explicit solution of the equation, which had not been given by the previous authors. The interested reader should consult Kerr & Dold's (1994)

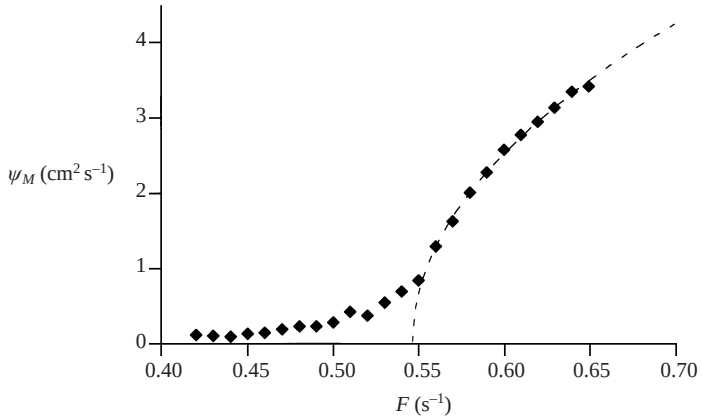

FIGURE 9. The instability threshold. The evolution of an order parameter (the maximum ψ_M of the streamfunction) as a function of the control parameter, the rotation frequency of the rollers.

article for the nonlinear analysis of the problem and the asymptotic development of the solutions.

4.2. *Explicit solution of the linearized problem*

The unstable modes are invariants along x and can be written using a streamfunction ψ:

$$v_x = \gamma x, \quad v_y = -\gamma y + \partial_z \psi, \quad v_z = -\partial_y \psi. \tag{4.2}$$

Neglecting the advection generated by the disturbances themselves the equation for the x-component of the vorticity is

$$\partial_t \omega_x = \gamma \partial_x (x\omega_x) + \nu \Delta \omega_x. \tag{4.3}$$

Since there is no advection of the vorticity along the z-axis the disturbance can be developed in Fourier modes along this direction:

$$\omega_x = \omega_0 f\left(\frac{y}{\ell}\right)\cos(kz) \tag{4.4}$$

with $f(0) = 1$ and $f''(0) = -1$.

As in the experiment the disturbance is thus a periodic array of counter-rotating vortices aligned along x, the stretching direction; ω_0 is the vorticity at the core of the vortices, k the wavenumber in the z-direction and ℓ the vortex typical size in the direction of the compression y. The vorticity is the opposite of the streamfunction's Laplacian. We can write:

$$\psi = \ell^2 \omega_0 g\left(\frac{y}{\ell}\right)\cos(kz) \tag{4.5}$$

with $g'' - (k\ell)^2 g = -f$. While g is defined up to a hyperbolic cosine it becomes unique if it has to vanish at infinity: $g(+\infty) = 0$. We first seek stationary solutions. Inserting ω_x of the form (4.4) in the vorticity equation (4.3) we get a differential equation for f:

$$f''(\zeta) + \frac{\gamma \ell^2}{\nu}\zeta f'(\zeta) + \ell^2\left(\frac{\gamma}{\nu} - k^2\right) f(\zeta) = 0. \tag{4.6}$$

Using the condition defining ℓ, $f''(0) = -1$, we get a relation among the stretching γ,

the viscosity ν, the core size ℓ and the core's ellipticity $k\ell$:

$$\frac{\nu}{\gamma} = \frac{\ell^2}{1 + k^2\ell^2}. \tag{4.7}$$

This relation is an expression of the equilibrium between the stretching which tends to concentrate the vortices and the viscosity which tends to diffuse their core. The size of the core is thus the length scale based on the stretching γ and the viscosity ν. With this constraint the differential equation for f depends on one single parameter, a Reynolds number Re^* based on the stretching and on the core size ℓ:

$$Re^* \equiv \frac{\gamma\ell^2}{\nu} = 1 + k^2\ell^2. \tag{4.8}$$

Because of the viscous equilibrium there can only be solutions for Reynolds number larger than 1. Introducing Re^*, the vorticity equation reduces to

$$f''(\zeta) + Re^*\zeta f'(\zeta) + f(\zeta) = 0. \tag{4.9}$$

As shown by H. K. Moffatt (private communication), with the change of variable $\xi = -\frac{1}{2}Re^*\zeta^2$, equation (4.9) reduces to the confluent hypergeometric equation:

$$\frac{\mathrm{d}^2 f}{\mathrm{d}\xi^2} + \left(\frac{1}{2} - \xi\right)\frac{\mathrm{d}f}{\mathrm{d}\xi} - \frac{1}{2Re^*}f = 0, \tag{4.10}$$

whose solution is the confluent hypergeometric function:

$$f(\zeta) = \Phi\left(\frac{1}{2Re^*}, \frac{1}{2}, -\frac{Re^*}{2}\zeta^2\right). \tag{4.11}$$

The limit $Re = 1$ corresponds to a wavenumber $k = 0$, i.e. to a constant-vorticity layer along the z-direction. The solution is then simply Gaussian, since $\Phi\left(\frac{1}{2}, \frac{1}{2}, -\frac{1}{2}\zeta^2\right) = \exp\left(-\frac{1}{2}\zeta^2\right)$. We thus recover the Burgers shear layer as a limit case. For $Re > 1$ both the velocity and the vorticity tend to zero at infinity. Far from the core the vorticity results from an equilibrium between stretching which tends to amplify it and advection which brings in weak vorticity from the outer regions:

$$f(\zeta) \propto \zeta^{-1/Re}. \tag{4.12}$$

For large values of the Reynolds number, i.e. for large aspect ratio $k\ell$, the flow should tend towards an array of vortices strongly elliptical along y. Note that the streamlines have a larger ellipticity than the isovorticity contours. This effect becomes stronger when the Reynolds number is close to 1. A complete discussion of the topology difference between the streamlines and the vorticity contours can be found in Moffatt, Kida & Ohkitani (1994). Experimentally, we measured a streamline aspect ratio of 1.75.

4.3. *Comparison with the experiment*

The results of this linear stability analysis can now be compared to the experimental results. The analysis of the infinite hyperbolic flow predicts its instability whatever the stretching γ. The eigenmodes are formed of arrays of vortices aligned in the direction of the stretching, as observed in the experiment. In the experiment however the instability exhibits a well-defined threshold which does not show up in this linear analysis where the unstable modes are subjected to only one constraint: the core size has to be larger than the viscous size. In the experiment, a geometrical constraint

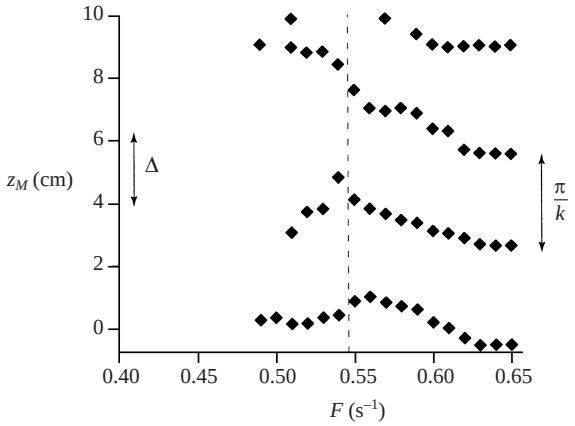

FIGURE 10. Evolution of the vortex positions z_M, defined by the streamfunctions extrema, as a function of the roller frequency F. Above the threshold, a well-defined wavelength is selected, which is of the order of the gap Δ between the rollers.

naturally appears: the transverse size of the vortex in the y-direction has to be smaller than the gap Δ and the transverse size in the z-direction smaller than the cell height h. The first mode which can appear, given these conditions, is thus $\ell \simeq \Delta$ and $kh \simeq \pi$ and corresponds to a very elliptical vortex of aspect ratio $k\ell \simeq \pi\delta/h \simeq 0.3$, a vortex so elliptical that it would be close to a shear layer along the z-axis.

In reality several vortices are formed at threshold showing that the constraining length-scale is the distance Δ separating the rollers and that vortex aspect ratio $k\ell \simeq 1$ is selected. Globally, the wavelength is selected similar to that observed in the Taylor–Couette flow: k has to be of the order of π/Δ (figure 10). Using the viscous equilibrium relation (4.7), the critical stretching has to satisfy approximately

$$\frac{\nu}{\gamma_c} = \frac{\ell^2}{1 + k^2\ell^2} \simeq \frac{1}{2k^2} \simeq \frac{\Delta^2}{2\pi^2}. \tag{4.13}$$

Or equivalently, the critical Reynolds number Re_c has to be of the order of

$$Re_c \simeq 2\pi^2 \simeq 19.7, \tag{4.14}$$

which is close to the measured one ($Re_c = 17.3 \pm 1.5$).

In order to compare the shape of the vortices observed experimentally to that predicted by the linear theory, we have to introduce the amplitude (figure 9), the measured wavenumber k (figure 10), the viscosity ν and the stretching γ in the previous formulas. The shape along the y-direction is then determined (ℓ is not to be adjusted). The velocity fields predicted by the linear theory are plotted in figure 11 for the same values of γ as in figure 8. Just above the critical Reynolds number, the middle line appears to be sinusoidal and, far above, the flow becomes dominated by the array of vortices. The shapes of the streamlines agree remarkably well with those measured experimentally. In particular, the vortex core aspect ratio, which is determined by the viscous equilibrium (and is thus not fitted) appears to be the same as that observed experimentally. This means essentially that the actual flow is determined by the competition between vortex stretching and viscous diffusion.

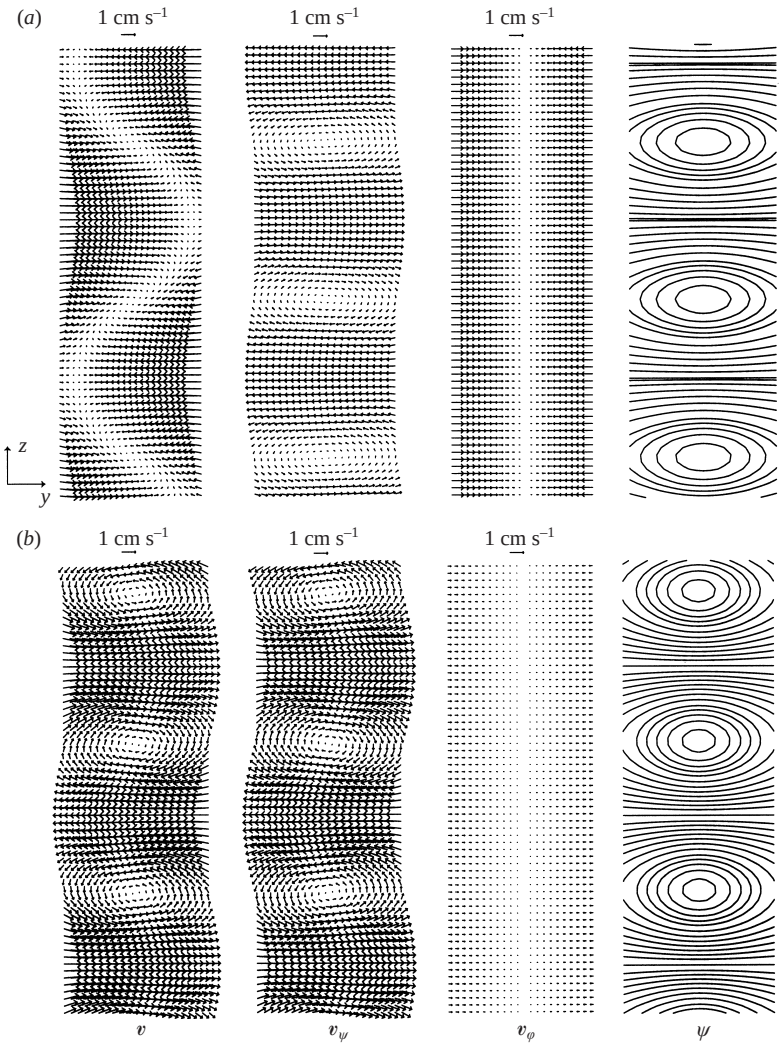

FIGURE 11. Velocity fields in the plane $x = 0$ predicted by the linear analysis for two Reynolds numbers located above the threshold: (*a*) $Re = 15.9$ ($F = 0.55$ Hz); (*b*) $Re = 19.1$ ($F = 0.65$ Hz). As for the experimental fields the velocity field $\boldsymbol{v}$ is given on the left and decomposed into a two-dimensional vortical component $\boldsymbol{v}_\psi$ (centre left) and an irrotational stretching part $\boldsymbol{v}_\varphi$ (centre right). The streamlines (iso-ψ) are shown on the right.

5. High Reynolds number experiments: the interaction between strain and vorticity in rotating regions

At high Reynolds number (in water), direct observation shows a turbulent flow which remains very anisotropic, at least at large scale. Coherent structures are still observed but they are much more intense, now looking like strong vortices preferentially aligned in the stretching direction. These vortices are disordered and transient, constantly forming and vanishing. A photograph of a cross-section of the flow in the plane perpendicular to the stretching direction is given in figure 12.

It is worth noting that the internal Reynolds number Re based on the stretching and on the gap Δ between the roller (equation (3.2)) is not very high but the external Reynolds number is. The maximum frequency we could achieve was $F = 12$ Hz. For

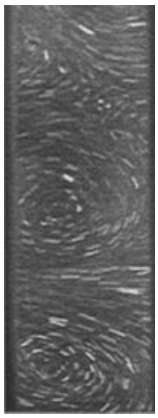

FIGURE 12. Close-up view of a cross-section of the flow in the median plane yOz of the cell (perpendicular to the stretching direction x) in the turbulent regime at $Re \simeq 1600$. Two vortices and a stagnation point can be seen.

this value, the internal Reynolds number is slightly larger 3000 while the Reynolds number based on the roller velocities and on their radius is of the order of 10^5.

We performed a series of measurements of the velocity profile $v_x(x)$ across the whole cell, in the stretching direction x (the measurement which gave us the value of the parameter γ (figure 4)). Below the instability threshold it is steady and independent of the position on the z-axis. At high Reynolds number the profile $v_x(x)$ fluctuates. For most of the time it is noisy due only to the turbulence of the fluid but retains a similar global profile. However, intermittently, the whole velocity gradient is strongly reduced for a short time. Since particles are present in the flow for the ultrasonic anemometry, it is possible to simultaneously measure the velocity profile and visualize the flow. This systematic comparison of the visual appearance of the flow with the corresponding measurements requires two observers: one to watch the flow itself, the second to look at the fluctuating profile on the computer screen. We were able in this way to observe that all the profiles having a weak gradient were those obtained at the precise moment when the core of a vortex passed in front of the probe (with its axis along the direction of measurement). In reverse we also checked that all the vortices passing the probe generated a weakening of the gradient.

The average profile is well defined: it is shown (at $F = 6\,\mathrm{Hz}$) by the open circles on the four plots of figure 13. The velocity gradient induced by the rollers is clearly visible; it is practically constant from $z = -45\,\mathrm{mm}$ to $z = +45\,\mathrm{mm}$, i.e. in the whole central region of the cell. Its value is $\gamma = 3.6\,\mathrm{s}^{-1}$, i.e. $0.6F$. Two instantaneous profiles taken at random times are shown for comparison on figure 13(a) (black circles). In spite of local turbulent fluctuations they exhibit the same global velocity gradient.

Since we could visualize the flow during the measurements, we also triggered instantaneous measurements of $v_x(x)$ at the exact moment when the axis of one of the turbulent vortices coincided with the axis of the ultrasonic probe. Two examples of such profiles are shown on figure 13(b) (black circles). The velocity gradient along the axis of a vortex is clearly weaker than the average gradient and of the order of $\gamma = 0.7\,\mathrm{s}^{-1}$ only.

6. Discussion: the dynamics of interaction between strain and vorticity

We can now return to turbulence. Our present results can contribute to a phenomenological interpretation of recently observed characteristics of turbulent flows.

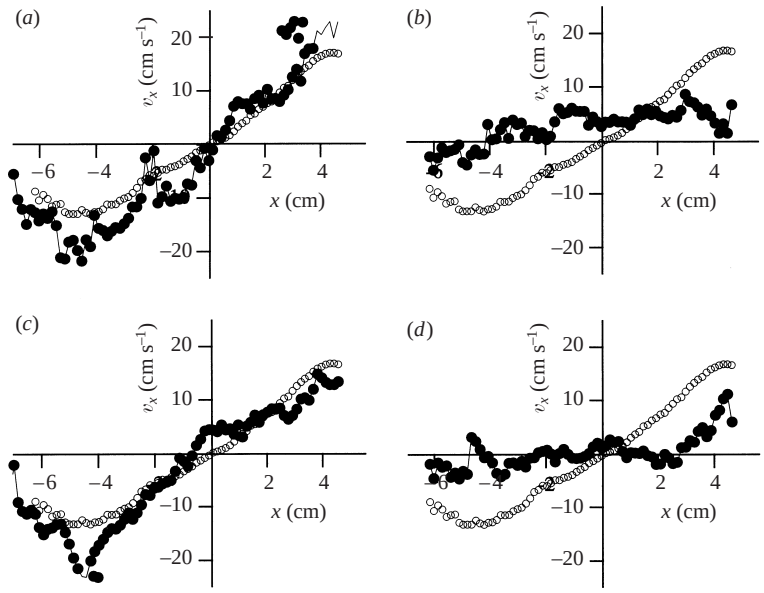

FIGURE 13. Longitudinal velocity profiles in the stretching direction at a rotation frequency of $F = 6$ Hz corresponding to a Reynolds number $Re \simeq 1600$. The origin of the abscissa is chosen in the centre of the cell and the narrowest gap between the cylinders is at $z = 4.5$ cm. The open circles show the mean velocity profile, obtained by averaging 1024 instantaneous profiles. (*a*) The black circles are two instantaneous profiles chosen at random times. (*b*) The black circles are two instantaneous profiles chosen at the precise time where the axis of a vortex coincided with the axis of the ultrasonic beam.

They are particularly related to the recently investigated pressure fluctuations and to the existence and dynamics of coherent structures. Statistically, a well-documented result is that the pressure fluctuations in a fully developed turbulent flow have an asymmetric distribution (Brachet 1991; Métais & Lesieur 1992; Fauve *et al.* 1993; Cadot *et al.* 1995). On the low-pressure side the probability distribution function has a long exponential tail due to rare events with large depressions. In contrast the high-pressure side has a shorter Gaussian tail. Because of the Poisson law (1.4) the pressure field reflects the spatial distribution of vorticity and strain. As shown experimentally by Cadot *et al.* (1995) the large depressions which are observed (at one point) as intermittent bursts are associated with intense vorticity filaments which have been observed directly both numerically (Siggia 1981; Tanaka & Kida 1993; Jimenez *et al.* 1993) and experimentally (Douady *et al.* 1991; Cadot *et al.* 1995). These structures form in a region with large stretching. Briefly they are coherent and rather straight, before finally disappearing in a kind of vortex breakdown.

6.1. *Regions of large strain and weak vorticity*

The intrinsic instability of the regions of pure strain had already been observed in the context of the formation of the secondary streamwise vortices of mixing layers (Lin & Corcos 1984; Neu 1984). Here we have investigated this instability in a controlled system and most of the characteristics that had been predicted theoretically have been observed. We thus have a situation in which vortices (low-pressure structures) are spontaneously formed in the regions of pure strain (high-pressure regions). While in such regions, the initial viscous flow contains almost no vorticity, it is unstable and transforms into a flow dominated by vortices. Where does the vorticity come from?

This paradox is only an apparent one: the hyperbolic flows are opened and suck in perturbations from the outside. Vorticity is thus captured, stretched and amplified, and feeds the instability.

The existence of a finite threshold in our experiment is directly linked with the finite extension of the experimental domain and with the corresponding limitation in wavenumber k. We believe that, in turbulence, whenever a region of nearly pure pure strain forms (by the interaction of neighbouring structures) it is intrinsically unstable. This instability process is likely to be responsible for the short lifetime and thus the scarcity of regions of pure strain and high pressure in turbulence.

This observation is in very good agreement with the results obtained on the statistics of enstrophy production in turbulent flows. From various conditional averaging Tsinober *et al.* (1999) have demonstrated that the enstrophy production is much larger in the regions dominated by strain than in those dominated by enstrophy.

6.2. *Regions of large vorticity and weak strain*

Our experiment, because of its geometry, seems to impose a well-determined longitudinal velocity gradient in the central region of the cell. This reproduces the conditions imposed on the theoretical solutions by Kerr & Dold (1994). In these solutions, as in all Burgers-like models (Burgers 1940), the stretching is an imposed field. The excellent agreement obtained between the experimentally observed flow and the theoretical one seems to validate this assumption in the low Reynolds number range.

At high Reynolds numbers however, as demonstrated in the previous section, the longitudinal velocity gradient is observed to be reduced in the vortex core region. Our hypothesis is that this effect is related to the two-dimensionalization due to the fast rotation near the core of axisymmetric vortices. In order to check this hypothesis we also investigated vortex stretching in a different configuration (Andreotti *et al.* 1997). We performed a variant of a classical experiment (Escudier 1984) in which a vortex is created in a cylindrical tank having a rotating disk at one end. In this experiment we introduced the possibility of pumping the fluid out of the cell through a hole located along the cell axis (the fluid being reinjected beneath the disk). When this suction is activated there is a transitory formation of a longitudinal velocity gradient along the vortex axis and intensification of this vortex. When the flow has become steady the vortex is very intense, and the velocity along its axis is large but the gradient of this velocity is drastically reduced (Andreotti *et al.* 1997).

In this latter experiment as well as in Taylor's four-roll mill, the observed effect is the same. The stretching of a vortex results in an intensification of its rotation. In turn this rotation tends to make the flow two-dimensional in the core and thus to oppose the variations of velocity in this region. This effect, as it reduces the velocity gradients, diminishes the stretching. There is thus a negative feedback of the vortices on the stretching which has generated them. This is a kind of Lenz law which had not been considered before.

The feedback mechanism is mainly that of Eckman pumping: when the stretching is inhomogeneous, it induces variations of the vortex rotation along its axis. The pressure gradient cannot balance the centrifugal force anymore, the latter having solenoidal part. As a consequence, the centrifugal force induces a radial flow in the part of the vortex where the rotation is the fastest and thus reduces the stretching in the vortex core. Globally, the vortex tends to reduce the stretching to which it is submitted, as soon as the stretching is localized in space. In another paper, we have investigated numerically (Abid *et al.* 2001) this mechanism of interaction. In particular, we have shown that the typical timescale of the feedback of rotation on

stretching scales as $L/U_{rotation}$ where L is the characteristic length over which the stretching is inhomogeneous (it is also the length of the vortex) and $U_{rotation}$ is the typical rotation velocity. The characteristic timescale of the vortex stretching is the inverse of the stretching γ. The ratio of the two,

$$B = \frac{U_{rotation}}{\gamma L}, \tag{6.1}$$

gives a non-dimensional parameter which characterizes the relative importance of the feedback mechanism and of the stretching process. For small B, the reaction can be neglected. In the limit case of homogeneous stretching, i.e. for Burgers-like vortices (Burgers 1940), L tends to infinity and B tends to zero: there is strictly no reaction. As soon as the rotation becomes important when compared to the stretching (if $B \gg 1$), the negative feedback of rotation on stretching must play a crucial role.

As a result, though the analytical solutions are good descriptions of the structures observed near the instability threshold, they fail to describe the situation at high Reynolds number because they do not take into account the negative feedback of rotation on stretching. In more recent models (Donaldson & Sullivan 1960; Gibbon, Fokas & Doering 1999; and Khomenko & Babiano 1999) the spatial homogeneity of the stretching has been relaxed, but it remains an imposed field. Our results show that in experimental situations the stretching is of finite extension and that the negative feedback of the vorticity on the stretching has drastic consequences. This effect should be taken into account in more realistic models of vortices.

This new mechanism has implications for turbulent flows. In all regions where vorticity is much larger than strain there is necessarily rotation, and this effect should appear. It is now well established by numerical simulations and experiments that most of the intense vorticity is concentrated in filament-like rotating structures. The two-dimensionalization of these vortices linked to their rotation provides a physical interpretation of the straightness of the vortex filaments observed in turbulent flows. This was observed experimentally by Cadot *et al.* (1995), demonstrated on theoretical grounds by Constantin, Procaccia & Segel (1995) and observed numerically by Galanti, Procaccia & Segel (1996). The corresponding reduction of the strain along the axis could also be responsible for the breakdown of the filaments which occurs ultimately.

It is often believed that the amplification of vorticity in turbulent flows is enhanced by nonlinear effects. This was proved wrong by Ohkitani (1998) who recently compared the stretching of a passive vector and that of the vorticity. The equations governing these two effects have similar linear terms and different nonlinear terms. The results of his numerical simulations demonstrate that, in a turbulent flow, the stretching of the vorticity is much weaker than that of passive vectors. The essential difference between the two is related to the relative orientations of the observed vector with the axes of strain. During its evolution the direction of the passive vector has no particular relation with the direction of the strain. In contrast, vorticity and strain being both constructed from the velocity derivatives have directions which are strongly related. Corresponding, as shown by Ohkitani (1998), the equation governing the passive vector evolution is linear while that concerning vorticity is nonlinear. In both cases the linear term has the same stretching effect on the passive vector and on vorticity. The weaker stretching of vorticity means that the nonlinear effects due to the alignments limit the stretching. We propose that the processes that we observe are the basis of the reduction of the vorticity stretching by nonlinearities. In the regions of high strain there is spontaneous collection and intensification of vorticity resulting in the formation of rotating regions. The rotation of these vortices generates

a negative feedback on stretching. These two effects could be the basic processes explaining Okhitani's result.

Finally, the negative feedback of rotation on stretching is a mechanism present in turbulence at all scales. At any scale, a coarse-grained vorticity and a coarse-grained strain tensor can be defined using for instance the velocity at the vertex of a tetrad (Chertkov, Pumir & Shraiman 1999). Like the actual vorticity and strain, the inertial effects can be interpreted as vortex stretching and centrifugal force at the scale under consideration. It was shown numerically by Chertkov *et al.* (1999) that *at all scales*, on the average, the pressure tends to counteract the effect of inertia but balances only part of it. This means that in rotating regions, the centrifugal force tends to expel the fluid from the centre of rotation and thus to reduce the stretching.

7. Conclusion

The instability of hyperbolic flows had already been investigated theoretically and was known to occur in the secondary instabilities of mixing layers. Here we have shown that a controlled version of this instability could be obtained in Taylor's four-roll mill experiment. In this set-up the flow which is stable at low Reynolds numbers, destabilizes by a supercritical bifurcation at a well-defined threshold and forms an array of counter-rotating vortices. The transverse velocity profiles of these vortices are in excellent agreement with those predicted by the theory of Kerr & Dold (1994). The instability threshold is well understood as resulting from the geometrical confinement of the flow.

We have also investigated this flow at high Reynolds number and the results thus obtained are relevant to the dynamics of the stretching of vorticity in turbulent flows. They can be summarized as follows:

(i) The regions of pure strain are highly unstable and are the locus of formation of organized vortices. This result is in good agreement with the observation by Tsinober *et al.* (1999) that these regions are statistically those of largest enstrophy production.

(ii) When strong vortices have formed the two-dimensionalization due to rotation reacts to reduce the stretching in their core. This nonlinear effect is in agreement with the weak enstrophy production observed in these regions by Tsinober (1998), with the alignments observed by Nomura & Post (1998) and with the results by Ohkitani (1998) on the nonlinear limitation of vortex stretching.

We are grateful to J. C. Sutra Fourcarde, H. Demaie and B. de Runz for their help during the experiment, and to J. Paret and O. Cardoso for the use of their PIV system. We wish to thank H. K. Moffatt who actually solved equation (4.9). A part of this article was written during a stay of Y.C. at the Isaac Newton Institute in Cambridge, the other while B.A. was participating in the turbulent program of the Institute for Theoretical Physics in Santa Barbara. Both institutes are thanked for their hospitality. This research was supported in part by the National Science Foundation under Grant No. PHY94-07194.

Appendix. Decomposition of the velocity field into a vortical and a stretching part

We want to decompose the velocity field in the central plane into a rotational part and a potential part:

$$v_y = \partial_z \psi + \partial_y \varphi, \quad v_z = -\partial_y \psi + \partial_z \varphi. \tag{A 1}$$

The main problem is that different sets of functions ψ and φ can be chosen corresponding to the same physical flow. If we consider a different potential φ' which has the same Laplacian as φ (so that $\Delta(\varphi' - \varphi) = 0$), there exists a second streamfunction ψ' which satisfies $\partial_z(\psi' - \psi) = -\partial_y(\varphi' - \varphi)$ and $\partial_y(\psi' - \psi) = \partial_x(\varphi' - \varphi)$. As a consequence, (φ, ψ) and (φ', ψ') correspond to the same velocity field. In this particular experiment, it would be arbitrary to use boundary conditions to determine ψ and φ.

Specifically, we wish to compare the velocity field measured experimentally to a hyperbolic flow disturbed by an array of vortices. This would mean a field of the form

$$v_y = \partial_z\psi - \gamma y, \quad v_z = -\partial_y\psi. \tag{A 2}$$

The best choice among the possible couples (φ, ψ) is that which minimizes the difference between the stretching part of the flow and a pure hyperbolic flow. Suppose that we know the couple (φ_0, ψ_0) which satisfies (A 1) in a rectangular region S together with the boundary condition $\varphi_0 = 0$. We want to find the potential φ and the stretching γ which minimizes the surface integral:

$$\int_S [(\partial_y\varphi + \gamma y)^2 + (\partial_z\varphi)^2]\mathrm{d}s \tag{A 3}$$

under the constraint that everywhere in the rectangle $\Delta(\varphi - \varphi_0) = 0$. The solution is easy to obtain: φ is the solution of $\Delta\varphi = \Delta\varphi_0$ with the boundary condition $\varphi = -\gamma y^2/2$ and γ is given by the integral relation

$$\gamma = \frac{\displaystyle\int_S -y\partial_y\varphi \mathrm{d}s}{\displaystyle\int_S y^2 \mathrm{d}s}. \tag{A 4}$$

In practice, an iterative procedure can be used to solve these coupled equations. A regular grid is used and the velocity derivatives are estimated by finite differences. We first find the field of the form (A 2) closest to the experimental measurements. To do this, we minimize with respect to $\psi_{j,k}$ and γ the usual likelihood functional L based on the differences between the model velocity field and the experimental one:

$$L = \frac{1}{2}\sum_{j,k} \frac{(v_y^{j,k+1/2} - (\psi_{j,k+1} - \psi_{j,k}) + \gamma j)^2 + (v_z^{j+1/2,k} + (\psi_{j+1,k} - \psi_{j,k}))^2}{\sigma_{j,k}^2}. \tag{A 5}$$

Note that each velocity measurement is weighted by the experimental standard deviation $\sigma_{j,k}$ measured for each mesh point. Note also that $\psi_{j,k}$ is defined up to a constant. We chose this constant in order that the maximum and minimum values of $\psi_{j,k}$ be opposite. This leads to a system of linear equations coupling the values of ψ at each grid point and γ which is solved numerically by a simple matrix inversion.

After this first step, we obtain an approximation of the measured velocity field in which the stretching field is spatially homogeneous. We then compute the difference $\delta\boldsymbol{v}$ between the initial field and its projection:

$$\delta v_y = v_y - \partial_z\psi + \gamma y, \quad \delta v_z = v_z + \partial_y\psi. \tag{A 6}$$

In most of the cases, this difference is already small compared to the velocity itself, meaning that expression (A 2) is a good approximation of the actual flow. We then find the potential field $\nabla\varepsilon$ closest to $\delta\boldsymbol{v}$ (in the least-square sense) and satisfying the boundary condition $\varepsilon = \varphi + \gamma y^2/2 = 0$ derived above.

Again we compute the difference between the total velocity field $\boldsymbol{v}$ and $\nabla\varepsilon$ and seek $\psi_{j,k}$ and γ minimizing the likelihood functional L. And again the best potential ε is determined. This process is iterated until convergence is achieved. In practice only three iterations of the type described above are necessary before obtaining a satisfactory decomposition (the rest being of the order of the noise). Adding the γ and ε contributions, the potential is finally $\varphi = -\gamma y^2/2 + \varepsilon$.

REFERENCES

Abid, M., Andreotti, B., Douady, S. & Nore C. 2001 Oscillating structures in a stretched-compressed vortex. *J. Fluid Mech.* (submitted).

Andreotti, B. 1999 Action et réaction entre étirement et rotation, du laminaire au turbulent. PhD Thesis report, Université Paris 7, Paris.

Andreotti, B., Douady, S. & Couder, Y. 1997 About the interaction between vorticity and stretching in coherent structures. In *Turbulence Modelling and Vortex Dynamics* (ed. O. Boratav & A. Erzan), pp. 92–108. Springer.

Aryshev, Y. A., Golovin, V. A. & Ershin, S. A. 1982 Stability of colliding flows. *Fluid Dyn.* **1**, 755–759.

Bentley, B. J. & Leal, L. G. 1986 A computer controlled four-roll mill for investigations of particle and drop dynamics in two-dimensional linear shear flows. *J. Fluid Mech.* **167**, 219–240.

Brachet, M. E. 1991 Direct simulation of three-dimensional turbulence in the Taylor-Green vortex. *Fluid Dyn. Res.* **8**, 1–8.

Burgers, J. M. 1940 Application of a model system to illustrate some points of the statistical theory of free turbulence. *Proc. Acad. Sci. Amsterdam* **43**, 2–12.

Cadot, O., Douady, S. & Couder, Y. 1995 Characterisation of the low-pressure filaments in a three dimensional turbulent shear flow. *Phys. Fluids* **7**, 630–646.

Cardoso, O., Marteau, D. & Tabeling, P. 1994 Quantitative experimental study of the free decay of quasi two-dimensional turbulence. *Phys. Rev.* E **49**, 454–460.

Chertkov, B., Pumir, A. & Shraiman, B. 1999 Lagrangian tetrad dynamics and the phenomenology of turbulence. *Phys. Fluids* **11**, 2394–2412.

Constantin, P., Procaccia, I. & Segel, D. 1995 Creation and dynamics of vortex tubes in three-dimentionnal turbulence. *Phys. Rev.* E **51**, 3207–3222.

Craik, A. D. D. & Criminale, W. O. 1986 Evolution of wavelike disturbances in shear flows: a class of exact solution of Navier-Stokes equations. *Proc. R. Soc. Lond.* A **406**, 13–26.

Criminale, W. O., Jackson, T. L. & Lasseigne, D. G. 1994 Evolution of disturbances in stagnation-point flow. *J. Fluid Mech.* **270**, 331–347.

Donaldson, C. D. & Sullivan, R. D. 1960 Behaviour of solutions of the Navier-Stokes equations for a complete class of three-dimensional viscous vortices. In *Proc. Heat Transfer & Fluid Mech. Inst.*, Stanford University.

Douady, S., Couder, Y. & Brachet, M. E. 1991 Direct observation of the intermittency of intense vorticity filaments in turbulence. *Phys. Rev. Lett.* **67**, 983–986.

Dunlap, D. & Leal, L. G. 1987 Dilute polystyrene solutions in extensional flows – Birefringence and flow modification. *J. Non-Newtonian Fluid* **23**, 5–48.

Escudier, M. P. 1984 Vortex breakdown: observations and observations. *Exps. Fluids* **2**, 189–196.

Fauve, S., Laroche, C. & Castaing, B. 1993 Pressure fluctuations in swirling turbulent flows. *J. Phys. Paris* II **3**, 271–278.

Fuller, G. G, Rallison, J. M., Schmidt, R. L. & Leal, L. G. 1980 The measurement of velocity gradients in laminar flow by homodyne light-scattering spectroscopy. *J. Fluid Mech.* **100**, 555–575.

Galanti, B., Procaccia, I. & Segel, D. 1996 Dynamics of vortex lines in Turbulent flows. *Phys. Rev.* E **54**, 5122–5133.

Gibbon, J. D., Fokas, A. S. & Doering, C. R. 1999 Dynamically stretched vortices as solutions of the 3D Navier Stokes equations. *Physica* D **132**, 497–510.

Jeong, J. & Hussain, F. 1995 On the identification of a vortex. *J. Fluid Mech.* **285**, 69–94.

Jimenez, J., Wray, A. A., Saffman, P. G. & Rogallo, R. S. 1993 The structure of intense vorticity in homogeneous isotropic turbulence. *J. Fluid Mech.* **255**, 65–90.

Kerr, O. S. & Dold, J. W. 1994 Periodic steady vortices in a stagnation-point flow. *J. Fluid Mech.* **276**, 307–325.

Khomenko, G. & Babiano, A. 1999 Quasi-three-dimensional flow above the Ekman layer. *Phys. Rev. Lett*. **83**, 84–87.

Kida, S. & Miura, H. 1998 Identification and analysis of vortical structures. *Eur. J. Mech.* B **17**, 471–488.

Lagnado, R. R. & Leal, L. G. 1990 Visualization of three-dimensional flow in a four-roll mill experiment. *Exps. Fluids* **9**, 25–32.

Lagnado, R. R., Phan Thien, N. & Leal, L. G. 1984 The stability of two dimensional linear flows. *Phys. Fluids* **27**, 1094–1101.

Leblanc, S. & Godeferd, S. 1999 An illustration of the link between ribs and hyperbolic instability. *Phys. Fluids* **11**, 497–499.

Lin, S. J. & Corcos, G. M. 1984 The mixing layer: Deterministic models of a turbulent flow. Part 3. The effect of plane strain on the dynamics of streamwise vortices. *J. Fluid Mech.* **141**, 139–178.

Métais, O. & Lesieur, M. 1992 Spectral large eddy simulation of isotropic and stably stratified turbulence. *J. Fluid Mech.* **239**, 157–194.

Moffatt, H. K., Kida, S. & Ohkitani, K. 1994 Stretched vortices – the sinews of turbulence; large Reynolds number asymptotics. *J. Fluid Mech.* **259**, 241–264.

Neu, J. C. 1984 The dynamics of stretched vortices. *J. Fluid Mech.* **143**, 253–276.

Nomura, K. K. & Post, G. K. 1998 The structure and dynamics of vorticity and rate of strain in incompressible homogeneous turbulence. *J. Fluid Mech.* **377**, 65–97.

Ohkitani, K. 1998 Stretching of vorticity and passive vectors in isotropic turbulence. *J. Phys. Soc. Japan* **67**, 3668–3671.

Ohkitani, K. & Kishiba, S. 1995 Nonlocal nature of vortex stretching in an inviscid fluid. *Phys. Fluids* **7**, 411–421.

Raynal, F. 1996 Exact relation between spatial mean enstrophy and dissipation in confined incompressible flows. *Phys. Fluids* **8**, 2242–2245.

Saffman, P. G. 1992 *Vortex Dynamics.* Cambridge University Press.

Siggia, E. D. 1981 Numerical study of small scale intermittency in three-dimensional turbulence. *J. Fluid Mech.* **107**, 375–406.

Tanaka, M. & Kida, S. 1993 Characterisation of vortex tubes and sheets. *Phys. Fluids* A **5**, 2079–2082.

Taylor, G. I. 1934 The formation of emulsions in definable field of flow. *Proc. R. Soc. Lond.* A **146**, 107–125.

Taylor, G. I. 1938 Production and dissipation of vorticity in a turbulent fluid. *Proc. R. Soc. Lond.* A **164**, 15–23.

Townsend, A. 1976 *The Structure of Turbulent Shear Flow*. Cambridge University Press.

Tsinober, A. 1998 Is concentrated vorticity that important. *Eur. J. Mech.* B **17**, 421–449.

Tsinober, A., Ortenberg, M. & Shtillman, L. 1999 On depression of non-linearity in turbulence. *Phys. Fluids* **11**, 2291–2297.

Tsinober, A., Shtillman, L. Sinyavskii, A. & Vaisburd, H. 1997 A study of vortex stretching and enstrophy generation in numerical and laboratory experiments. *Fluid Dyn. Res.* **21**, 477–494.